Competitive removal of textile dyes from solution by pine bark-compost in batch and fixed bed column experiments

Khaled Al-Zawahreh [a], María Teresa Barral [b], Yahya Al-Degs [c], Remigio Paradelo [b,*]

[a] Department of Earth Sciences and Environment, Prince El-Hassan bin Talal Faculty for Natural Resources and Environment, The Hashemite University, Zarqa 13133, Jordan
[b] CRETUS, Department of Soil Science and Agricultural Chemistry, University of Santiago de Compostela, 15782 Santiago de Compostela, Spain
[c] Department of Chemistry, Faculty of Science, The Hashemite University, P.O. Box 330127, Zarqa 13133, Jordan

A B S T R A C T

Compost from pine bark has been previously suggested as an effective low-sorbent for different classes of textile dyes, although the existing studies have been performed in non-competitive batch conditions, so the effect of competition or adsorption in continuous-flow conditions has not been assessed. In this work, the removal of Basic Violet 10 (BV10) and Direct Blue 151 (DB151) by pine bark compost from single and bi-solute mixtures has been studied in batch and fixed-bed column experiments. Adsorption capacity of pine bark compost was three times higher for BV10 than for DB151 in batch conditions, where competition reduced the uptake of both dyes, with competition factors of 0.63 for DB151 and 0.82 for BV10. Dye adsorption capacity was lower in column than in batch tests, with 112.6 and 34.7 mg g^{-1} for BV10 and DB151, respectively, versus 127.1 and 42.1 mg g^{-1} in batch conditions. The presence of both dyes in solution also reduced their affinities with respect to non-competitive conditions in column tests, with saturation capacities of 71.6 mg g^{-1} for BV10 and 16.8 mg g^{-1} for DB151. The effect of competition between dyes was higher in columns than in batch conditions, with competition factors of 0.76 for BV10 and 0.59 for DB151. The column biosorbent was effectively regenerated using ethanol, thus enabling reuse in the practical application of compost for textile dye removal. The concentration of dyes in the eluted ethanol was higher than the influent concentration, what would give compost value for pre-concentration of textile dyes.

© 2022 The Author(s). Published by Elsevier B.V. This is an open access article under the CC BY license (http://creativecommons.org/licenses/by/4.0/).

1. Introduction

A large number of synthetic dyes are commercially available and currently employed in numerous applications. These dyes are classified by their source (natural and manufactured), chemical structure (indigoid, anthraquinone, azo, polymethine, nitro and nitroso, and polycyclic aromatic carbonyl), and substrate use (reactive, acidic, basic, and disperse) (Raval et al., 2017). Cationic and direct dyes are widely employed in the textile industry, with advantages such as high color brightness, a broad color palette, reasonable substantivity and cost-effectiveness (Raval et al., 2017). Industrial coloring, however, is frequently the source of water contaminants that can be harmful (predominantly water-soluble poisonous,

carcinogenic, and/or mutagenic) to people and other life forms, as well as having unappealing aesthetic consequences. In addition, textile dye effluents and tannery wastewaters contribute to the build-up of chemical oxygen demand and biological oxygen demand in water bodies (Durai and Rajasimman, 2011; Saharimoghaddam et al., 2019; Sy et al., 2019), making them unsuitable for other secondary purposes. It is also worth noting that the majority of synthetic dyes are resistant to water, light and chemical substances (Raval et al., 2017; Bilal et al., 2019). As a result, it is critical to design systems for their removal from wastewater.

It is already well known that adsorption is a highly recommended methodology for removing dye molecules from effluent streams, due to advantages such as high efficiency, ease of application, adaptability and economic viability (Tahira et al., 2016). In general, solid adsorbents are classified into three categories (Patel, 2019): (a) Synthetic adsorbent: Different porous materials with high adsorption capabilities are produced in the laboratory using various procedures. The expensive production process is the main disadvantage of these adsorbents. (b) Natural adsorbent: Natural materials such as plant roots, leaves, and agricultural waste are dried, crushed, and washed with distilled water before being utilized as an adsorbent for target pollutants. Although natural adsorbents are inexpensive, its adsorption capacity is rather limited. (c) Semi-synthetic adsorbent: Natural materials are activated biologically, chemically or physically to produce a highly porous surface. The main benefits of these adsorbents are low cost, high efficiency, no chemical or biological sludge as by-products, and possible absorbent. In this regard, composted organic residuals have recently been investigated as a potential natural material for dyes removal from solution (Paradelo et al., 2019, 2020; Al-Zawahreh et al., 2021, 2022). Composting organic waste is the most sustainable way to avoid leachate and greenhouse gas emissions after disposal or landfilling. Composting reduces the initial waste volume by up to 65% and yields a nutrient-rich end product that can be used as organic amendment (Ayilara et al., 2020).

Besides agricultural uses of compost, increasing attention is being paid to its remediation applications, including removal of textile dyes (Anastopoulos and Kyzas, 2015). The published research indicates the good performance of composts for removing different classes of dyes, with high affinity for cationic dyes compared to anionic ones (Kausar et al., 2018; Benkhaya et al., 2020; Al-Zawahreh et al., 2021). In this sense, the adsorption capacity of compost for basic dyes has been observed to be 10 to 20 times higher than for reactive and acid dyes (Paradelo et al., 2019; Al-Zawahreh et al., 2021). However, this has been tested in non-competitive batch conditions, with no systematic studies for competitive removal available and very few in column conditions (Kamarudzaman et al., 2015). In general, very few studies have reported competitive adsorption of textile dyes by any biosorbent (Al-Ghouti et al., 2016; Issa et al., 2017; Yu et al., 2019). Taking this into account, the current work has the following objectives:

(i) to assess the effect of competition on textile dye removal from water by pine bark compost,

(ii) to assess the performance of pine bark compost as biosorbent in continuous-flow conditions, and

(iii) to understand the factors that influence the performance of pine bark compost for dye removal.

2. Materials and methods

2.1. Compost

The compost used as biosorbent was produced in an industrial composting facility in the region of Galicia (Spain) and derived from the abundant and unused pine bark residues. The compost was generated via aerobic composting of pine bark in windrows and supplied by the company Costiña Orgánica (A Coruña, Spain). It presents a high content of organic matter (95.3%) and acidic nature, with pH in water of 5.3 and a point of zero charge (pH_{PZC}) of 4.4. It presents low electrical conductivity (0.98 dS m^{-1}), low nutrient contents (0.01, 0.32, and 0.93% for N, P and K, respectively), and very low levels of Pb and Zn, 7.4 and 33.8 mg kg^{-1}, respectively. Cation exchange and anion exchange capacity values are 26.2 and 4.6 cmol$_c$ kg^{-1}, respectively. N$_2$ adsorption–desorption analysis indicated a specific surface area of 22.4 m^2 g^{-1} and a mean pore size diameter of 135 Å. Further information about characteristics of the adsorbent, including FTIR spectra, can be found in previous publications (Paradelo et al., 2020; Al-Zawahreh et al., 2021, 2022). For the adsorption tests, the sample was crushed and sieved at a particle size 250–500 μm.

2.2. Textile dyes

Two textile dyes were selected for the study, belonging to basic and direct dye classes. Basic Violet 10 (BV10, also known as Rhodamine B) and Direct Blue 151 (DB151) were obtained from Panreac (Barcelona, Spain) and Sigma–Aldrich® (USA) chemicals, respectively. The pKa values of the dyes, determined from the half-point of pH-V_{NaOH} titration plot of 0.010 M dye solution and chemical structures are shown in Fig. 1. BV10 has no azo bond and can form a zwitterion at pH 3, while DB151 has a large hydrophobic skeleton with two azo bonds, polar groups (N–H and O–H) and two ionizable sulfonate groups.
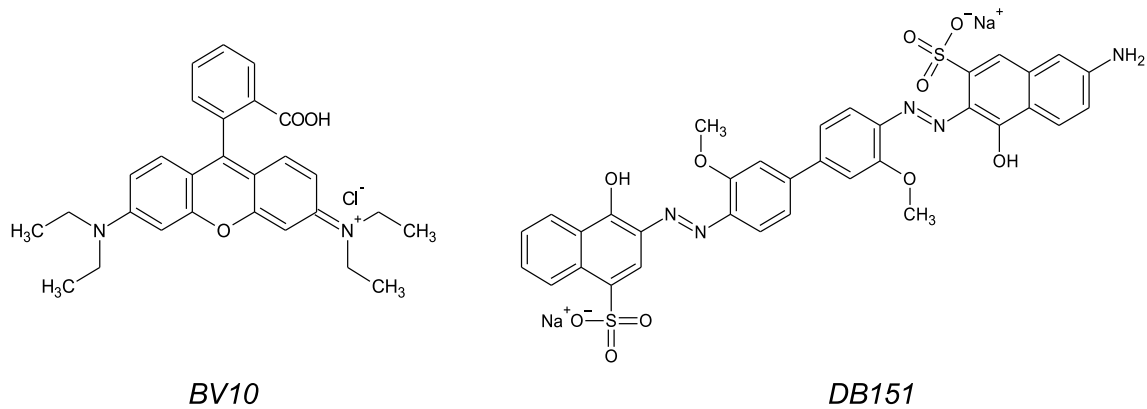
Fig. 1. Chemical structures of Basic Violet 10 (BV10) (pKa 3.70) and Direct Blue 151 (DB151) (pKa 2.68).

2.3. Adsorption isotherms of single and bi-solute systems

Adsorption isotherms (at 25 ± 1 °C) for both dyes were determined individually in batch experiments using the concentration–variation method. Samples of 0.50 g (±0.01 g) of compost (particle range 250–500 μm) were added to 50.0 mL of solutions containing different concentrations of dyes (5.0–2000 mg L^{-1} for BV10 and 5.0–700 mg L^{-1} for DB151). To have equal chance for dyes adsorption from solution, competitive tests were carried using equal molar concentration of both dyes. The tests were performed at pH 3.0 to maximize the affinity of both dyes toward compost, based on the results of previous works (Al-Zawahreh et al., 2021). The suspensions were sealed and placed in a thermostated shaker (GFL, Germany) for 24 h, the equilibrium time as determined from earlier kinetic studies (Al-Zawahreh et al., 2021). After equilibrium, the supernatants were separated and dye concentrations were determined by measuring absorbance values of the solutions using a double-beam spectrophotometer (Thermo evolution 100 electro Corporation, USA) at 547 nm and 554 nm for BV10 and DB151, respectively. For single-solute solution, dye concentration was estimated from Beer's law, while for bi-solute solution modified Beer's law was solved at the maximum wavelengths of both dyes. Blank solutions, containing no compost, were also included in the study. The amount of dye absorbed, q$_e$ (mg g^{-1}) is estimated as follows:

$$q_e = (C_0 - C_e) \cdot V / m \tag{1}$$

where C$_0$ is the initial solute concentration (mg L^{-1}), C$_e$ is the equilibrium concentration in the extract (mg L^{-1}), V is the volume of solution (L), and m is the mass of adsorbent (g). Adsorption isotherms were performed in triplicate and the average values were reported.

2.4. Fixed bed column adsorber tests for single and bi-solute systems

In addition to adsorption isotherms, column or fixed bed adsorber experiments are often required for testing practical application. For this, a glass column with internal diameter of 1.0 cm was filled with a known amount of pine bark compost. In order to provide a uniform inlet flow, a layer of 3.0 mm-glass beads was placed at the top of the packed compost. The column tests were carried out by pumping the dye solution through the column in downward flow mode, using a peristaltic pump (Smith and Nephew Watson-Marlow, England). All experiments were conducted at 25.0 °C and pH 3.0. The effect of various operational factors including flow rate (10–30 mL min^{-1}), bed-depth height (5.1–17.8 cm) and influent dye levels (50–150 mg L^{-1}) were investigated. The column was considered to be essentially exhausted when the effluent concentration reached 90% (i.e., C$_{eff}$/C$_{inf}$ = 0.9) of initial concentration and the breakthrough point at C$_{eff}$/C$_{inf}$ = 0.01. The effluent solutions from the column were collected at different intervals and dye concentrations analyzed as described above. In addition to single dye uptake, bi-solute competitive adsorption was examined at different bed-depths of adsorber. For the binary mixtures, dyes were quantified as outlined earlier.

2.5. Regeneration of compost fixed-bed adsorber

Desorption tests can clarify the nature of adsorption and the potential recycling of the exhausted compost. If the adsorbed dyes can be eluted by distilled water, then the dye is attached to the adsorbent by weak bonds. Hence, desorption tests were performed for batch and column systems using different solvents including water. In the batch study, 0.1 M sulfuric acid, 0.1 M acetic acid, or ethanol were added to the dye-loaded compost and shaken for 5 h. The suspensions were centrifuged at 5000 rpm for 5.0 min and the supernatants were analyzed for dye content. The chemical reagent

with the highest dye recovery was selected for desorption in the column test. In this case, the 17.8-cm columns saturated with dyes were regenerated by passing the solvent through them at a flow rate of 5.0 mL min^{-1}, a lower flow rate than that used in the adsorption tests for a better elution from compost. Effluents were recovered and analyzed as explained above, until the eluted dye content was below 1.0 mg L^{-1}.

2.6. Mathematical modelling

2.6.1. Adsorption isotherms

Different adsorption models, including two and three parameter models, were adjusted to experimental data in order to predict the maximum uptake capacity, formation of multilayer adsorption, variability of active sites, porosity, and heterogeneity of sorbent. Among known models, only Langmuir and Freundlich were found to be applicable. Langmuir equation has the following form:

$$q_e = \frac{Q_L K_L C_e}{1 + K_L C_e} \tag{2}$$

where Q_L (mg g^{-1}) and K_L (L mg^{-1}) are respectively the maximum adsorption capacity and the affinity constant of the dye toward the compost. The model assumes equal-energy active sites, no interaction with adsorbed solutes, and one mono-layer coverage. The Freundlich model expression defines the heterogeneity of the surface as well as the exponential distribution of the active sites and the active sites energies:

$$q_e = K_F C_e^{1/n} \tag{3}$$

where K_F (L^n mg^{1-n} g^{-1}) is the Freundlich constant and can indicate uptake capacity, while $1/n$ (dimensionless) measures the favorability of the process, and both are system specific constants. Competitive adsorption was assessed by estimating the competition factor (CF) as follows (Issa et al., 2017):

$$CF = Q_{max}(bi\text{-}solute\text{-}system)/Q_{max}(single\text{-}solute\text{-}system) \tag{4}$$

where Q_{max} (bi-solute-system) and Q_{max} (single-solute-system) are the maximum retention capacities estimated from single and bi-solute systems, respectively. In case of positive competition, CF is higher than unity and adsorption is enhanced by the other solutes. For CF = 1, adsorption takes place without competition. The general case is CF<1, meaning that solute affinity is reduced due to negative competition with other solutes. The relative error of prediction (REP%) was used as a criterion to select the optimum model as equilibrium data was fitted by more than one model. REP% is estimated as follows:

$$REP\% = 100 \cdot \sqrt{\frac{\sum_{i=1}^{n}(q_{i,pred} - q_{i,act})^2}{\sum_{i=1}^{n}\left(q_{i,act}\right)^2}} \tag{5}$$

where $q_{i,pred}$, $q_{i,act}$, and n are predicted adsorption value, actual adsorption value, and number of experimental points, respectively. Lower REP% indicates better model fitting to the data.

2.6.2. Mass transfer zone and breakthrough curve

The relation between the nature of breakthrough curve and fixed-bed adsorption is adequately explained by the mass transfer zone model (Walker and Weatherley, 2000). The pollutant is removed most rapidly and effectively in a mass transfer zone (MTZ) at the upper fraction of adsorbent during the initial step of the interaction. This is due to the higher volume of adsorbent and lower amount of adsorbate present in these upper layers, allowing adsorbate to easily escape in the lower strata of the bed and no adsorbate runoff from the adsorbent at the first stage. As a result, a MTZ forms at the front of the column where adsorption occurs, and goes until it reaches the adsorber end, when the effluent solute concentration begins to rise in the aqueous phase (Faust and Aly, 1987; Walker and Weatherley, 2000). The faster adsorption kinetics, the shallower is the MTZ. The time needed for mass transfer zone (TMTZ) to develop and move down to the end of column adsorber is estimated as V_{ex}/u, where V_{ex} and u are total volume of solution needed for saturation and volumetric flow rate, respectively. The height of mass transfer zone (HMTZ) often depends on adsorption rate and flow rate of solution and is estimated as follows:

$$HMTZ = H \cdot (t_{ex} - t_b)/t_{ex} \tag{6}$$

where H is bed-depth (cm), t_{ex} is the time needed for adsorber exhaustion (min), and t_b is the time for breakthrough (min).

The breakthrough curve plots the ratio of effluent to influent dye concentration (C_{eff}/C_{inf}) as a function of process time (t) or treated volume (V). At a certain saturation point, the total capacity of the column is calculated as follows:

$$q_{bed} = \frac{u \cdot C_0}{m \cdot 1000} \int_{t=0}^{t=t_{saturation}} \left(1 - \frac{C_{eff}}{C_{inf}}\right) dt \tag{7}$$

4

where u is the feed flow rate (mL min^{-1}), C_{eff} is the effluent concentration at time t (mg L^{-1}), C_0 is the inlet concentration (mg L^{-1}) and $t_{saturation}$ is the time required for the bed to become saturated (min) at $C_{eff}/C_{inf} = 0.9$. Two common models were used to model the curves: the Thomas model was used to estimate dye saturation values and influence of competition, while bed depth service time (BDST) model was used to estimate service time of the adsorber at different bed-depths. The Thomas model allows to calculate the rate constant and maximum solid-phase concentration of adsorbate on adsorbent and it is used to establish breakthrough curves over long service time and often applied to model dye removal in column experiments (Negrea et al., 2020). It is based on the premise that rate driving forces follow second-order reversible reaction kinetics and that there is no axial dispersion in Langmuir adsorption–desorption kinetics (Thomas, 1944). Hence, it has been frequently adopted to study adsorbents of high capacity at dynamic conditions. The Thomas equation is linearly presented as follows:

$$ln(\frac{C_{inf}}{C_{eff}} - 1) = \frac{K_{Th}q_{Th}m}{u} - K_{Th}C_0t \tag{8}$$

where C_{inf} is the concentration of influent solution (mg L^{-1}); C_{eff} is the solution concentration at time t in the effluent solution (mg L^{-1}); K_{Th} is the Thomas rate constant, (L mg^{-1}min^{-1}); q_{Th} is the equilibrium solute uptake per gram of compost (mg g^{-1}); m is the mass of adsorbent (g); u is the volumetric flow rate (mL min^{-1}).

The BDST model, proposed by Bohart and Adams (1920), offers a simple approach and rapid prediction of adsorber design and performance (McKay and Bion, 1990; Al-Degs et al., 2009). In terms of process concentrations and adsorption factors, this model is based on the relationship between bed depth and service time. This model assumes that the adsorption rate is proportional to both the residual capacity of sorbent and the concentration of the adsorbing solute. The linear form of the model is as follows:

$$\ln \left(\frac{C_{inf}}{C_{eff}} - 1 \right) = \ln \left(e^{k_a N_{oH}\frac{}{u}} - 1 \right) - k_aC_0t \tag{9}$$

where C_{inf} (mg L^{-1}) is the inlet dye concentration and C_{eff} (mg L^{-1}) is the maximum acceptable limit concentration which could be at 50% exhaustion, t is the fix-bed service time (s) and H is the bed-depth (m). N_0 is the column adsorption capacity (mg L^{-1}), u is the volumetric flow rate (m^3 s^{-1}) of solution, k_a is the BDST rate constant (L mg^{-1} s^{-1}). As the exponential term in Eq. (9) is usually much larger than unity, then the relation is reduced to:

$$t = \frac{N_0}{C_{inf}u}H - \frac{1}{k_aC_{inf}} \ln(\frac{C_{inf}}{C_{eff}} - 1) \tag{10}$$

From the slope and intercept, both N_0 and k_a can be calculated. At 50% breakthrough ($C_{inf}/C_{eff} = 0.5$), the second term on the right-hand side of Eq. (10) is reduced to zero, generating the following simplified equation:

$$t_{0.5}=N_o/C_ou \cdot H \tag{11}$$

A plot of $t_{0.5}$ (service time at 50% breakthrough or $C_{eff}/C_{inf} = 0.5$) versus H should yield a straight line with a slope equal to $N_0/C_0 \cdot u$, and this slope represents the time required to exhaust a unit length of the adsorber under the applied experimental variables. In fact, Eq. (10) can be used to estimate column service time at C_{eff}/C_{inf} range 0.1–0.5 or saturation% from 10–50. Finally, the adsorbent utilization factor (η) relates the total capacity achieved in adsorber (q_{bed}) with the total capacity obtained in equilibrium batch isotherm (Q_{max}) and therefore represents the amount of active sites that are not utilized in the adsorber:

$$\eta = q_{bed}/Q_{max} \tag{12}$$

3. Results and discussion

3.1. Dye adsorption from single and bi-solute mixtures in batch condition

As a previous step to the dynamic column tests, equilibrium adsorption of BV10 and DB151 in single and bi-solute systems was investigated. The curves obtained are shown in Fig. 2 and the parameters of the models and quality of fit are given in Table 1. Both competitive and non-competitive adsorption of the two dyes presented L2-type isotherm shapes, according to Giles and Smith classification (Giles et al., 1960), in agreement with the literature (Al-Degs et al., 2007; Al-Ghouti et al., 2016; Issa et al., 2017). This reflects a high affinity between BV10 and DB151 and compost at low concentrations and a saturation of the sorbent at high concentrations, as well as a limited effect of competition between BV10 and DB151 toward active sites in the compost. In theory, competition between dyes should increase with concentration, thus disturbing the typical L2-isotherm, but this has not been observed here.

As shown in Table 1, Langmuir model outperformed Freundlich model for presenting equilibrium data and also showed good prediction of saturation for both dye adsorption systems, with REP% values lower than 10 in all cases. The good applicability of Langmuir model to present bi-solute systems can be attributed to the basic assumption of this model of no interaction between sorbates. Although Freundlich model described adequately single-solute systems (REP% 9.2–2.4), it was not able to predict competitive adsorption in bi-solute systems (REP% 11.4–12.7). In the case of the Langmuir model,
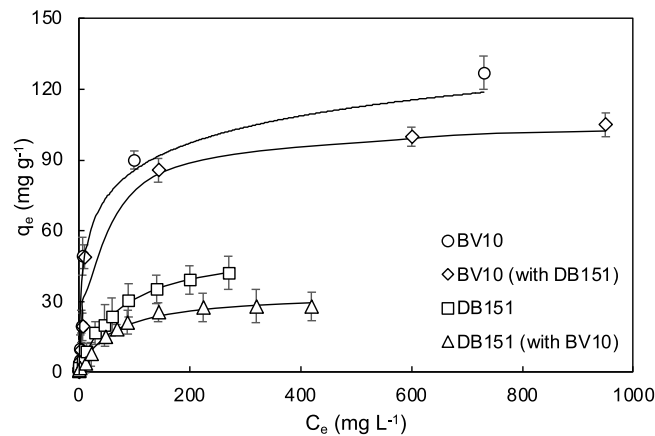
Fig. 2. Single and bi-solute adsorption isotherms of dyes by pine bark derived compost. Competitive adsorption tests were carried out using equal molar concentration of both dyes in the solution.

Table 1
Isotherm parameters for competitive adsorption of BV10 and FD151 by compost.

System	Q_{exp}	Langmuir			Freundlich			Competition factor
		Q_L	K_L	REP%	K_f	n	REP%	
BV10	127.0	127.1	0.039	1.5	13.40	2.78	2.4	0.82
BV10 (with BD151)	105.0	104.6	0.044	5.2	12.01	3.03	12.7	
DB51	42.1	53.9	0.0134	2.9	3.02	2.10	9.2	0.63
DB151 (with BV10)	29.0	33.8	0.0166	6.1	3.21	2.61	11.4	

Q_{exp}: experimental saturation estimated from isotherms. Q_L: Langmuir maximum capacity (mg g^{-1}); K_L: Langmuir constant (L g^{-1}); K_F: Freundlich constant (L^n mg^{1-n} g^{-1}); n: Freundlich coefficient.

K_L can be an indicator of the favorability of adsorption through the determination of the dimensionless separation factor: $R_L = 1/(1+K_L C_o)$, with R_L values between 0 and 1 indicative of favorable adsorption. The R_L values obtained here were in the range of 0.99–0.96, also indicating a favorable retention of dyes in all systems.

Indeed, compost showed a high affinity for both dyes, with a combined adsorption capacity of 138 mg g^{-1} in the bi-solute system, which was larger than the capacities for each dye in single-solute systems. In binary systems, variable competitive effects exist among dyes for active sites, as shown by the competition factors estimated using the saturation values predicted by the Langmuir model. With a competition factor of 0.63, uptake of DB151 was more affected in bi-solute system than BV10, with a competition factor of 0.82.

Compared to other materials, the adsorption capacity of CPB for BV10 (127 mg g^{-1}, Table 1) is in the same range of the values obtained with more expensive synthetic adsorbents like graphene oxides (155 mg g^{-1}) and activated carbon (264 mg g^{-1}, Yu et al., 2013), and higher than the values reported for natural adsorbents such as zeolite (13.2 mg g^{-1}), kaolinite (46.1 mg g^{-1}, Yu et al., 2013), bentonite (98 mg g^{-1}, Namasivayam et al., 2001), or banana peels (10 mg g^{-1}, Oyekanmi et al., 2019). The values are also higher than those reported for other composts, for example 27.2 mg g^{-1} obtained for a sewage sludge and plant residue compost (Jóźwiak et al., 2013) or 36.1 mg g^{-1} for MSWC compost (Al-Zawahreh et al., 2021). Comparing the performance of the compost for DB151 is more difficult due to the scarcity of adsorption studies with this specific molecule, although our previous work has shown that CPB has higher adsorption capacity for this dye than municipal solid waste compost (Al-Zawahreh et al., 2021). In summary, composted pine bark is very efficient for dye removal compared to other sorbents, specially taking into account its low production cost, which is around 20–30 $ m^{-3}.

In previous works, the adsorption mechanism of different types of dyes (including basic and direct dyes) on compost has been investigated by assessing the effect of pH and ionic strength changes on adsorption and by studying FTIR spectra of dye-loaded composts (Paradelo et al., 2020; Al-Zawahreh et al., 2021). The results of these studies have shown that surface functional groups like carboxylic acids are involved in adsorption and that, in general, electrostatic interaction is an important mechanism of interaction in both cationic and anionic dyes. However, it cannot be the only mechanism behind dye removal. At the pH tested here, compost would present a net positive charge (pH$_{solution}$ < pH$_{PZC}$), but dyes would present charges of different sign: positive for BV10 and negative for DB151. Thus, electrostatic interaction is stronger for DB151 than for BV10, and if this was the main mechanism of interaction, adsorption capacity would also be higher for DB151, which was not the case. Considering the complex structure of the dye molecules and compost, the contribution of other mechanisms such as hydrophobic–hydrophobic and dipole–dipole forces should be envisaged to explain dye sorption under unfavorable charge conditions. Indeed, hydrophobic interaction is likely to play an important role, specially taking into account the high organic matter content of the compost (95%) and the large bands of polysaccharides and aromatic rings observed in the FTIR spectra of the compost (Al-Zawahreh et al., 2021).

Table 2

Parameters of Thomas model, height of mass transfer zone (HMTZ), and time mass transfer zone (TMTZ) estimated at different operational conditions.

Factor	Value	Model parameters				
		BV10				
		K_{Th}	q_{Th} (mg g^{-1})	HMTZ (cm)	TMTZ (h)	REP%
Bed-depth[a] (cm)	5.1	0.00055	24.9	4.6	2.3	9.4
	12.7	0.00044	72.8	5.1	7.3	8.5
	17.8	0.00037	102.8	6.5	12.8	7.4
Flow rate[b] (ml min^{-1})	10	0.00037	102.8	6.5	12.8	7.4
	20	0.00082	75.4	5.1	4.6	7.8
	30	0.00094	58.5	4.9	2.1	6.5
Concentration[c] (mg L^{-1})	50	0.00044	57.4	3.1	13.9	9.8
	100	0.00037	102.8	6.5	12.8	7.4
	150	0.00029	112.6	7.2	9.1	7.5
		DB151				
Bed-depth[a] (cm)	5.1	0.00081	22.2	2.2	1.9	6.1
	12.7	0.00072	26.6	3.8	3.0	8.0
	17.8	0.00055	31.8	4.1	4.6	6.4
Flow rate[b] (ml min^{-1})	5	0.00031	36.5	8.7	8.1	8.3
	10	0.00055	31.8	4.1	4.6	6.4
	15	0.00056	25.4	2.4	2.6	9.2
Concentration[c] (mg L^{-1})	50	0.00061	21.2	3.9	5.1	9.3
	100	0.00055	31.8	4.1	4.6	6.4
	150	0.00047	34.7	5.1	2.7	7.8

[a]Flow rate 10 ml min^{-1}; Initial concentration 100 mg L^{-1}.
[b]Bed-depth 17.8 cm; Initial concentration 100 mg L^{-1}.
[c]Bed-depth 17.8 cm; flow rate 10 ml min^{-1}.

3.2. Removal of dyes from single-solute solution by fixed-bed adsorber

The breakthrough curves of dyes at different experimental conditions are provided in Figs. 3 and 4, whereas the results of their analysis using Thomas model and MTZ parameters are provided in Tables 2 and 3. The performance in the fixed-bed column is shown by the evolution of the ratio between the effluent dye concentration and the influent concentration in the influent (C$_{inf}$/C$_{eff}$). Since mass transfer rates were finite, the removal of BV10 and DB151 by the compost adsorber at different operational conditions presented diffuse breakthrough curves with a typical S-shape of variable steepness, which have also been reported for large dye molecules adsorbed onto porous durian peel waste (Thuong et al., 2019). The curves presented a varying degree of steepness, in agreement with previous works by Al-Degs et al. (2009) and Han et al. (2009). Deformed S shapes have been reported for reactive dyes adsorption onto activated carbon, which is attributed to slow interaction in the system (Han et al., 2009). Moreover, the shape of breakthrough curve is also sensitive to the tested parameter, for instance, steeper S-curves are often reported at high flow rate and short bed-depth (Patel, 2019).

Bed depth. Figs. 3A and 4A show the breakthrough curves of BV10 and DB151 at different bed heights, at fixed flow rate and influent dye concentration. Dyes uptake increased with bed height from 5.1 to 17.8 cm, due to the increment in surface area of adsorbent, which provided more active sites for the adsorption process as well as longer contact times of interaction. In general, steeper breakthrough curves are obtained with smaller bed depth, indicating faster adsorption kinetics, shorter breakthrough time, and fast column saturation. The curves obtained for the lowest bed-depth tested (5.1 cm) were steeper, with earlier breakthrough and faster equilibrium times in contrast with the curves obtained at the highest bed-depth (17.8 cm), with longer breakthrough time and equilibrium times. Rate of adsorption process, as indicated from Thomas model, was reduced by increasing bed-depth. For instance, increasing bed-depth from 5.1 to 17.8 cm resulted in 32 and 37% rate reductions in K_{Th} value for BV10 and DB151, respectively. The reduction in adsorption rate at higher bed-depth is correlated with the time needed to develop MTZ for each bed-depth. As shown in Table 2, longer TMTZ values were reported with longer bed depths and for both dyes. For BV10, time needed to create MTZ and movement along the adsorber was 12.8 h for 17.8 cm depth and only 2.3 h for 5.1 cm bed depth. Hence, adsorption rate of BV10 was slower (K_{Th} 0.00037) at longer bed depth. On the other hand, higher saturation capacity is expected at longer MTZ. For BV10, saturation capacity increased 4-times by bed depth and this is attributed to the increment of MTZ with bed depth (Table 2). Compared to BV10, the faster kinetics of DB151 (K_{Th} 0.00055–0.00088) was attributed to lower time needed to create MTZ (2.1–4.6 h) and faster breakthrough times (Fig. 4A). Higher column saturation was also reported for DB151, which is attributed to higher HMTZ.

The early breakthrough time (estimated from the treated volume and flow rate) also increased with bed height: the estimated breakthrough times for BV10 were 11.2, 283.4, and 573.4 min for 5.1, 12.7 and 17.8 cm, respectively. The
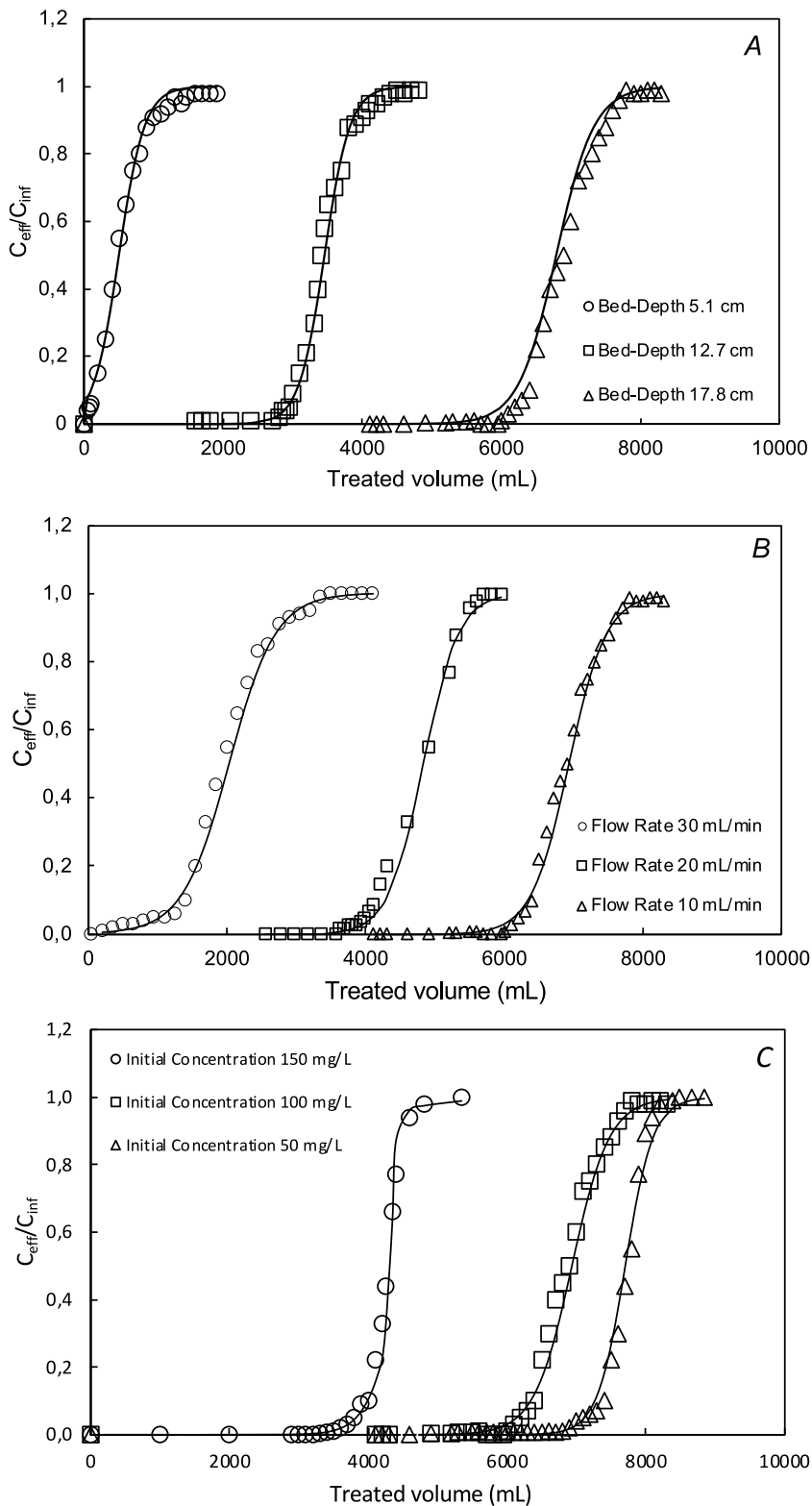
Fig. 3. Breakthrough curves of BV10 removal by compost adsorber (25 °C) at different operational factors.
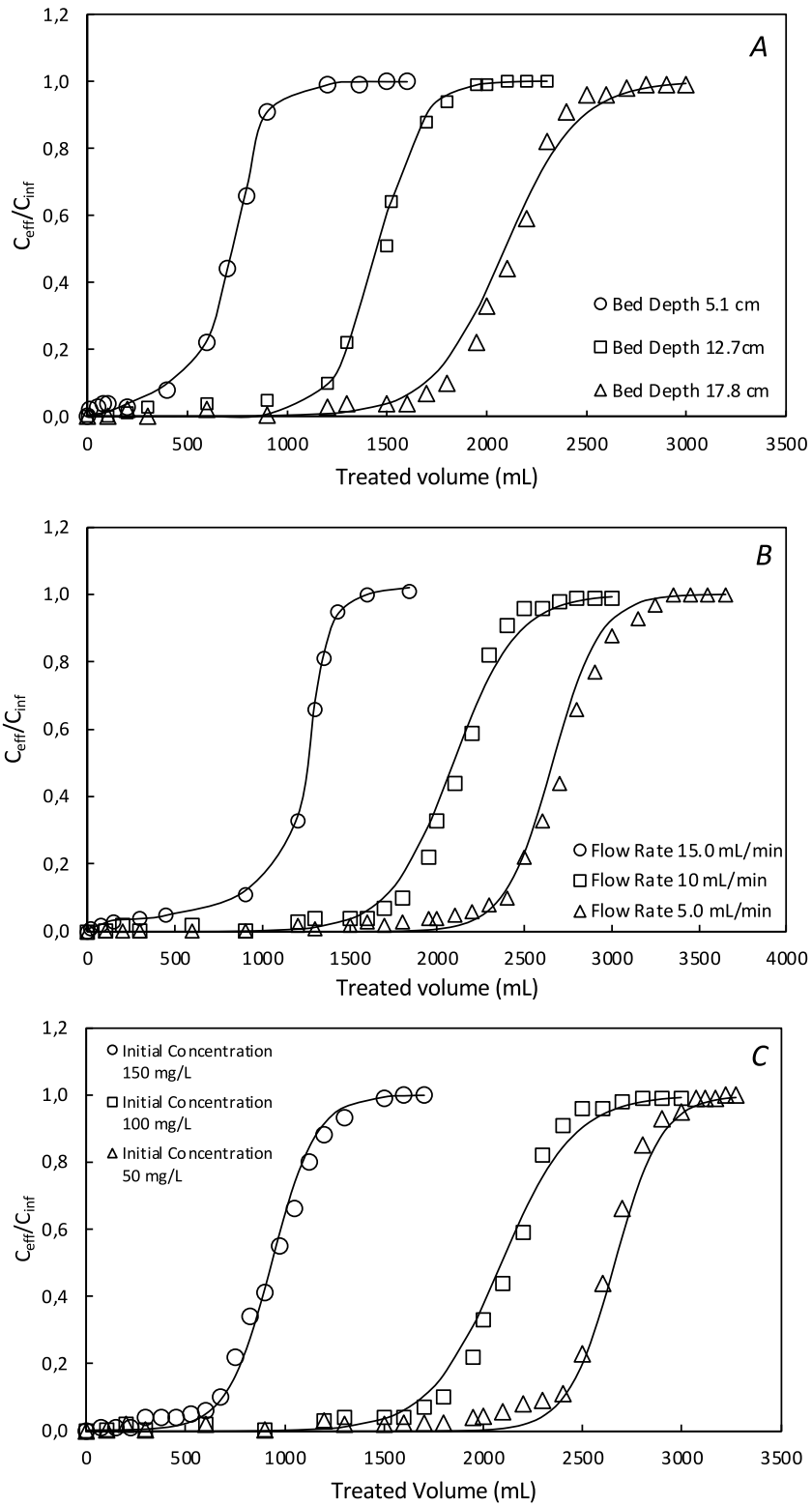
Fig. 4. Breakthrough curves of DB151 removal by compost adsorber (25 °C) at different operational factors.

Table 3

Bed capacity at $C_{eff}/C_{inf} = 0.9$, treated volumes at $C_{eff}/C_{inf} = 0.01$, and utilization factor (η) estimated at different operational parameters.

Factor	Value	Model parameters			
		BV10			
		V (L) 90%	V (L) 1.0%	q_{bed} (mg g^{-1})	η
Bed-depth[a] (cm)	5.1	1.4	0.3	23.9	0.19
	12.7	4.3	2.0	68.7	0.54
	17.8	7.61	4.52	97.5	0.77
Flow rate[b] (ml min^{-1})	10	7.61	4.52	97.5	0.77
	20	5.33	3.28	71.1	0.56
	30	3.51	0.61	53.9	0.42
Concentration[c] (mg L^{-1})	50	8.11	6.80	52.3	0.41
	100	7.61	4.52	97.5	0.77
	150	5.63	3.25	119.4	0.94
		DB151			
Bed-depth[a] (cm)	5.1	1.02	0.22	19.4	0.36
	12.7	1.71	0.85	24.3	0.45
	17.8	2.51	1.09	29.4	0.55
Flow rate[b] (ml min^{-1})	5	2.92	1.82	34.4	0.64
	10	2.51	1.09	29.4	0.55
	15	2.09	0.53	23.4	0.43
Concentration[c] (mg L^{-1})	50	3.12	1.89	19.4	0.36
	100	2.51	1.09	29.4	0.55
	150	1.12	0.34	24.6	0.46

[a]Flow rate 10 ml min^{-1}; Initial concentration 100 mg L^{-1}.

[b]Bed-depth 17.8 cm; Initial concentration 100 mg L^{-1}.

[c]Bed-depth 17.8 cm; flow rate 10 ml min^{-1}.

experimental data were fairly presented by Thomas model with REP% less than 10 in all cases (Table 2), which indicated that adsorption capacity increased to reach 102.8 and 31.8 mg g^{-1} for BV10 and DB151, respectively, at 17.8 cm depth. Thomas model predicted maximum column saturation. while in turn Eq. (7) estimates 90% saturation of column capacity, what explains the higher capacities obtained by the former model. The treated volumes at breakthrough point (i.e., 1% saturation point) also increased with bed depth (0.3, 2.0, and 4.5 liter for 5.1, 12.7 and 17.8 cm, respectively, for BV10. The same is true for DB151, for which it was observed an increase from 0.1 to 1.5 liter by increasing bed-depth from 5.1 to 17.8 cm. The adsorbent utilization factors (η) ranged from 0.19–0.77 for BV10 and 0.36–0.55 for DB151 (Table 3). Higher values of η indicate better utilization of compost adsorbent under dynamic conditions. However, running these tests with large columns (i.e., longer than 17.8 cm) was not experimentally practical as very high pressures were needed to reach the needed flow rates (10–30 mL min^{-1}). Hence, 17.8 cm was the optimum bed-depth under the tested operational parameters.

Flow rate. The results of the experiments to assess the influence of flow rate on the performance of compost adsorber are provided in Figs. 3B and 4B. In general, the shapes of breakthrough curves of BV10 were steeper than those obtained for DB151, what can be attributed to higher affinity of BV10 by compost and higher flow rates in BV10 column runs. For BV10, the breakthrough times estimated from treated volumes at $C_{inf}/C_{eff} = 0.01$ were 81.7, 377.4 and 608.3 min at 30, 20, and 10 mL min^{-1}, respectively, with exhaustion times ($C_{inf}/C_{eff} = 0.90$) of 334.5, 566.3, and 772.3 min at 30, 20 and 10 mL min^{-1}, respectively. Similar behavior was observed for DB151, but breakthrough times were notably lower. Longer exhaustion points at low flow rates are due to longer contact times leading to higher uptake by the sorbent, whereas at a higher flow rate conditions are further from equilibrium and adsorption affinity decreased due to lower residence time of the solute in the column and lower diffusion of dye into the pores of compost. The parameters of Thomas model (Table 2) indicated higher adsorption rate at high flow rates, while saturation capacity was notably reduced. For example, adsorption rates of BV10 were 0.00037, 0.00082, and 0.00094 L mg^{-1}min^{-1} and saturation capacities were 102.8, 75.4, and 58.5 mg g^{-1}, at flow rate of 10, 20, and 30 mL min^{-1}, respectively. The same trend was reported for DB151 but with lower rates and capacities. In fact, the high variations of HMTZ and TMTZ with flow rate was expected as both parameters were notably reduced at flow rate. The large reduction in HMTZ (25%–72% for both dyes at higher flow rate) can reflected the large reductions in their saturation values and volume of treated volumes upon exhaustion (Tables 2 and 3). On the other hand, the 70%–80% reduction of TMTZ with flow rate can explain the faster uptake of solutes with flow rate and this was also confirmed with high increase of K_{Th} with flow rate. The higher affinity of BV10 compared to DB151 at dynamic conditions reflects the favorable interaction of cationic dyes compared to anionic dyes, as consistently observed in compost-dye experiments (Paradelo et al., 2019; Al-Zawahreh et al., 2021, 2022). Treated volumes at saturation point $V_{0.9}$ were reduced for BV10 (50%) and DB151 (25%). For both dyes, saturation values were reduced by increasing flow rate, what negatively affected utilization factors, also decreasing down to 0.42 and 0.43 for BV10 and DB151, respectively, at

flow rate 30 mL min^{-1}. Consequently, for a more efficient utilization of compost adsorber, the columns should be operated at flow rates of 10 mL min^{-1} or lower.

Influent concentration. To address the effect of influent dye concentration on its uptake by compost adsorber, the initial concentration was increased from 50 to 150 mg L^{-1} while keeping the flow rate at 10 mL min^{-1} and bed depth 17.8 cm. Figs. 3C and 4C display the breakthrough curves of BV10 and DB151 at different influent concentrations. For both dyes, fast breakthrough happened at increasing influent dye concentrations, with breakthrough times at 1.0 and 90.0% saturation notably reduced. In general, the curves obtained at different concentrations have identical shape with comparable steepness at 50% saturation. For BV10 (Fig. 3C), the breakthrough times at $C_{inf}/C_{eff} = 0.01$ were 372.7, 609.6 and 712.4 min at initial concentration 150, 100 and 50 mg L^{-1}, respectively. However, for the same dye, the exhaustion times at $C_{inf}/C_{eff} = 0.90$ were 554.3, 766.5, and 837.8 min at concentration 150, 100 and 50 mg L^{-1}, respectively. The same behavior was observed for DB151, but breakthrough times were notably lower (Fig. 4C).

At initial interaction in adsorber, adsorption was fast due to availability of large number of active sites. Then, increasing dye concentration results in a higher driving force to overcome mass-transfer resistance in liquid phase and the bed saturated quickly leading to faster breakthrough and lower treated volume. Thomas model, which adequately presented the breakthrough curves for both dyes at different concentrations, indicated that adsorption rate slightly decreased with increasing dye influent concentrations. For BV10, adsorption rates were 0.00044, 0.00037, and 0.00029 L mg^{-1} min^{-1}, with saturation capacities of 57.4, 102.8, and 112.6 mg g^{-1} at dye concentrations of 50, 100, and 150 mg L^{-1}, respectively. The same trend was observed for DB151, but with capacities 21.2–34.7 mg g^{-1} (Table 2) over the tested concentration range. In fact, the parameters of MTZ can be helpful to explain the higher column saturation and lower rate by increasing feed concentration. For BV10, HMTZ increased from 3.1 to 7.2 cm (56% increment) and reflected the high column saturation at high concentration. As indicated in Table 3, running column tests for both dyes at 150 mg L^{-1} improved utilization factor, which increased up to 0.94 for BV10 and 0.46 for DB151, while resulted in large reductions (30%–60%) in treated volumes at exhaustion point for both dyes. Although utilization factor was increased but this is not practically enough considering the unjustifiable reduction in treated volume. It is worth noting that the utilization factor did not significantly changed with concentration, as was the case for bed depth and flow rate. This was attributed to a higher range of variation in q_{bed} with flow rate and bed depth, compared to dye concentration.

Overall, the optimum conditions for single-dye uptake by compost adsorber can be determined as those that led to the maximum η values (i.e., maximum compost utilization in column). With utilization factors of 0.77 and 0.55, the optimum conditions for sequestering both dyes would be: bed depth 17.8 cm, flow rate 10 mL min^{-1} and influent concentration 100 mg L^{-1}. Although a higher utilization factor (0.94) was reported for BV10, this was achieved at a very high influent concentration (150 mg L^{-1}) that may result in earlier column breakthrough. For DB151, a high utilization factor (0.64) was achieved at slow flow rate 5.0 ml min^{-1} (Table 3) and this may be not practical for real application, as the process would require excessive time.

3.3. Competitive removal by compost adsorber and bed depth service time

The breakthrough curves of bi-solute removal by adsorber and parameters for Thomas model, mass transfer zone (MTZ), and service time are shown in Fig. 5 and Table 4.

BV10. Most adsorption parameters were negatively affected by competition with DB151 in the dynamic system. In general, competition with DB151 reduced notably breakthrough points for the bed depth 12.7 and 17.8 cm, with a maximum reduction in breakthrough point of 36% for 17.8 cm, whereas comparable breakthrough point was observed using 5.1 cm (Fig. 5). For the same bed depth, reaction rate (K_{Th}) decreased for bi-solute systems, likely as a consequence of the reduction on HMTZ. As expected, saturation values of BV10 were reduced for each bed depth in 36%, 39%, and 25% for 5.1, 12.7 and 17.8 cm, respectively. The lower reduction for the 17.8 cm bed depth is mainly due to sufficient availability of active sites for both competing dyes. However, at smaller depth, the number of active sites will be limited and this will affect negatively saturation capacity at dynamic conditions. The interaction between dyes was not involved, as anticipated from the typical S-shape breakthrough curves of competitive systems. Both HMTZ and TMTZ decreased and the maximum reduction was reported for the short bed 5.1 cm, 30 and 50%, respectively. Removal of both dyes has consumed large number of active sites, as indicated for the high reduction in utilization factors to reach 0.12 only for 5.1 cm bed depth. Finally, the estimated competition factors for BV10 were 0.58, 0.64 and 0.76 for 5.1, 12.7, and 17.8 cm, respectively, indicating that the dye faced a strong competition with DB151 at the short bed depth 5.1 cm. The competition factors of BV10, 0.58–0.76, estimated from dynamic test, are lower than the one obtained in batch conditions, 0.82 (Table 1), due to longer contact time in the latter.

DB151. In general, the shape of breakthrough curves of DB151 for single and bi-solute systems is S-type (Fig. 5), with lower steepness compared to BV10 that could be attributed to its lower surface affinity at dynamic conditions. The highest steepness in breakthrough curves of DB151 were reported for 5.1-cm depth, due to shorter contact time in addition to negative competition with high-affinity BV10 dye. Because of intense competition with BV10 for active sites, the curves indicated very fast breakthrough (faster than those reported for BV10) and for all tested bed depths. The fastest breakthrough time was reported for 5.1 cm. Undoubtedly, dynamic removal of DB151 in presence of BV10 is not feasibly especially at small bed-depth. Column saturation values were reduced in the presence of BV10 and also dependent on bed-depth. The reduction was 40% for 17.8 cm depth and reached to 61% for 5.1 cm as indicated in Table 4. Due to negative
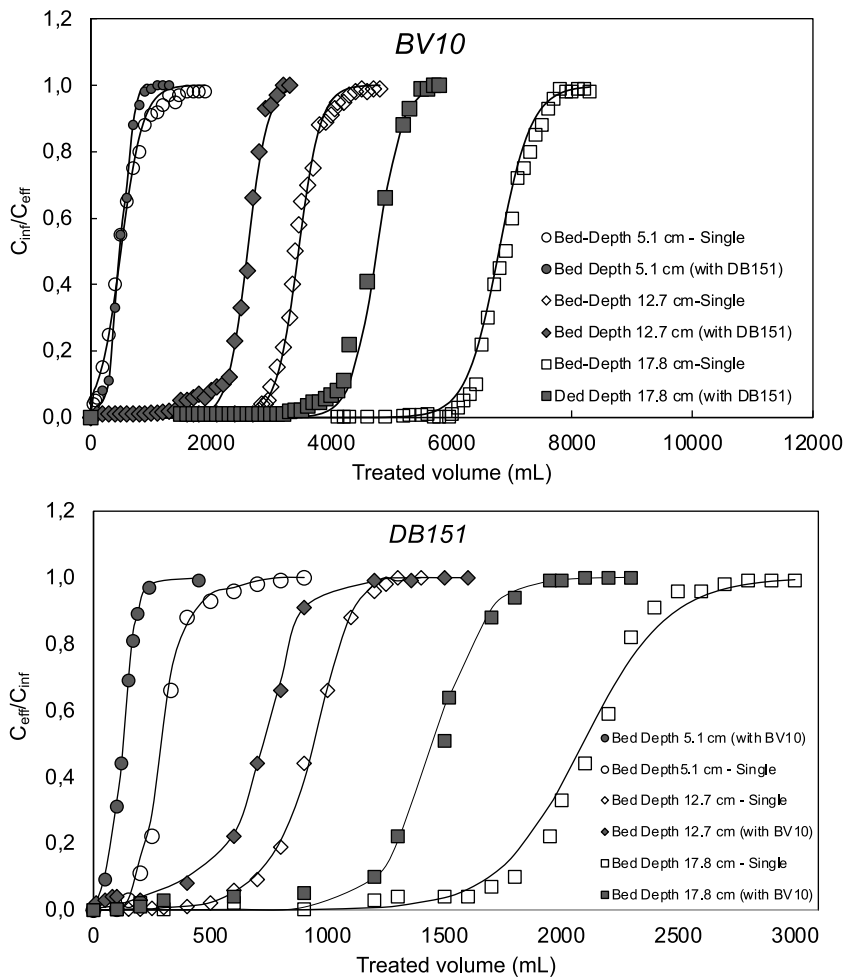
Fig. 5. Breakthrough curves of dyes for single and bi-solute (competitive) systems at different bed-depths at 25 °C. Flow rate 10 mL min^{-1}; initial concentration 100 mg L^{-1} for both dyes.

Table 4
Parameters of Thomas model, mass transfer zone (MTZ), and service time (50% saturation) for single and bi-solute uptake collected at different bed-depth adsorber. Flow rate 10 mL min^{-1}; initial concentration 100 mg L^{-1} for both dyes; 25 °C. Values in parenthesis are utilization factors.

	Bed depth (cm)	Parameters of Thomas Model and MTZ										Service time $t_{0.5}$ (h cm^{-1})	
		BV10					DB151						
		K_{Th}	q_{Th} (mg g^{-1})	REP%	HMTZ (cm)	TMTZ (h)	K_{Th}	q_{Th} (mg g^{-1})	REP%	HMTZ (cm)	TMTZ (h)	BV10	DB151
Single	5.1	0.00055	24.9(0.20)	9.4	4.6	2.3	0.00081	22.2(0.52)	6.1	2.2	1.9		
	12.7	0.00044	72.8(0.57)	8.5	5.1	7.3	0.00072	26.6(0.63)	8.0	3.8	3.0	0.75	0.23
	17.8	0.00037	102.8(0.81)	7.4	6.5	12.8	0.00055	31.8(0.75)	6.4	4.1	4.6		
Bi-solute	5.1	0.00014	16.3(0.12)	8.3	3.2	1.4	0.00018	8.7(0.21)	4.5	1.1	0.4		
	12.7	0.00021	43.9(0.51)	6.7	4.2	4.9	0.00032	11.6(0.27)	7.6	2.5	2.1	0.51	0.11
	17.8	0.00028	77.5(0.61)	9.1	6.0	9.1	0.00041	18.8(0.45)	6.4	3.1	3.1		

influence of BV10, HMTZ and TMTZ were notably reduced: by 51 and 79%, respectively, for 5.1 cm depth, making mutual dye uptake unpractical at small bed depths. Competition factors for DB151 at different depths were 0.39, 0.46, 0.59 for 5.1, 12.7, and 17.8 cm, respectively, which reflected the strong competition of BV10 (CF 0.58–0.76). As was the case for BV10, DB151 faced a higher competition under dynamic conditions than under batch conditions (CF 0.63, Table 1).

The bed-depth service time (BDST) model for dyes uptake was employed to get a better assessment of compost adsorber in single and bi-solute systems. This model is applied for the description of the initial part of the breakthrough curve, from 10 up to 50% exhaustion only (Chen et al., 2006). Analysis of adsorption data of single and bi-solute systems at different bed depths by BDST model is also shown in Table 4. Column service time for single dye uptake was notably
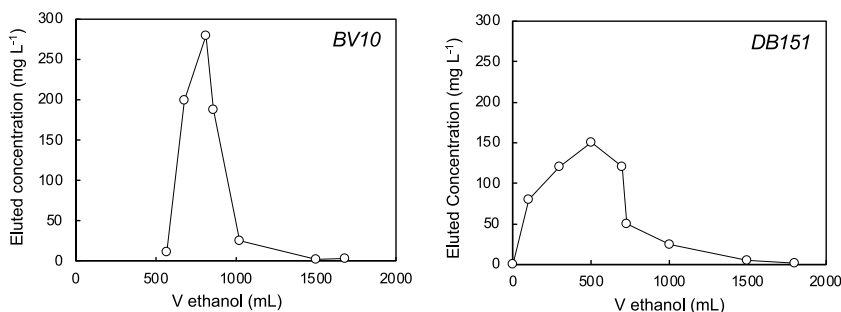
Fig. 6. Elution curves of BV10 and DB151 from compost fixed-bed adsorber (conditions: flow rate = 5 ml min^{-1}, bed height = 17.8 cm).

higher for BV10 than for DB151, and decreased in bi-solute systems, from 0.75 h cm^{-1} for BV10 alone down to 0.51 h cm^{-1} in the presence of DB151, and from 0.23 h cm^{-1} for DB151 alone down to 0.11 h cm^{-1} in the presence of BV10. Similar findings have been described earlier in the literature (Tan et al., 2008; Sharma and Foster, 1995).

3.4. Desorption of dyes from column adsorber

Among the solvents tested for regeneration of column adsorber, ethanol was the most effective in the preliminary batch studies. In the case of BV10, percentages of desorption were 11.3% for 0.1 M sulfuric acid, 21.5% for 0.1 M acetic acid and 56.4% for ethanol, whereas for DB151 those values were 14.6%, 21.5% and 49.7%, respectively. The high efficiency of ethanol for elution is likely due to higher solubility of the dyes in ethanol than in water, as reported previously (Al-Zawahreh et al., 2022). Consequently, elution of dyes from column adsorber was performed using ethanol (Fig. 6). Both dyes were effectively eluted using ethanol, although different volumes were needed for complete elution: 1570 mL for BV10 and 2000 mL for DB151. The maximum concentration of eluted dyes reaches 150 and 280 mg L^{-1} for BV10 and DB151, respectively, this is, significantly higher than influent dye concentration (100 mg L^{-1}). This implies that compost could also be potentially used to preconcentrate textile dyes.

3.5. Practical applications and future research prospects

The results of this work provide useful information for practical application of compost for dye removal: the column study with continuous flow is important for real scale operation, whereas the study of competition between dyes is useful for real textile wastewaters, where dyes of different classes can happen simultaneously. Besides, results show that ethanol could be used for compost regeneration or preconcentration of dyes from textile streams after adsorption. Future research in this topic should be oriented toward producing further information for practical application at real scale. This should involve studies about the influence of the presence of other pollutants typical of textile wastewaters, such as heavy metals, in the efficiency of dye removal. Another line of research would deal with potential modifications of the compost to increase their performance. These could include washing to remove excessive amounts of soluble organic matter, which can affect negatively the dye removal process (Toptas et al., 2014), temperature-mediated activation by boiling (Paradelo et al., 2009), or charring (Yang et al., 2016). Finally, research on sorbent regeneration and reuse should also be performed, studying different substances as eluents, as well as the effect of their concentration or other physicochemical parameters on dye desorption.

4. Conclusions

The performance of a pine bark compost for removal of textile dyes BV10 and DB151 was assessed in single and competitive conditions, with special attention to continuous flow fixed bed conditions. Maximum dye removal capacity in column conditions were 55%–77% of the batch equilibrium capacity. For bi-solute solution, a high competition among dyes was observed, which was stronger in dynamic/column conditions compared to batch mode. Due to competition for active sites, column utilization of available capacity was reduced to 45%–61% and service time was reduced from 0.75 to 0.51 h cm^{-1}. Removing DB151 in the presence of BV10 under dynamic condition may be not practical unless considering large bed depths. Utilization factors were highly reduced for bi-solute solution, indicating that full utilization of compost was not possible under dynamic column conditions. Column regeneration by ethanol was practical especially for preconcentration of both dyes from textile streams.

CRediT authorship contribution statement

Khaled Al-Zawahreh: Methodology, Validation, Formal analysis, Data curation, Writing – original draft, Writing – review & editing, Visualization, Project administration. **María Teresa Barral:** conceptualization, Methodology, Resources, Writing – review & editing, Supervision, Project administration. **Yahya Al-Degs:** Methodology, Validation, Writing – review & editing. **Remigio Paradelo:** conceptualization, Methodology, Validation, Investigation, Resources, Writing – review & editing, Visualization, Supervision, Project administration, Funding acquisition.

Declaration of competing interest

The authors declare that they have no known competing financial interests or personal relationships that could have appeared to influence the work reported in this paper.

Acknowledgments

References

Al-Degs, Y.S., Khraisheh, M.A.M., Allen, S.J., Ahmad, M.N., 2009. Adsorption characteristics of reactive dyes in columns of activated carbon. J. Hazard. Mater. 165, 944–949.

Al-Degs, Y.S., Khraisheh, M.A.M., Allen, S.J., Ahmad, M.N., Walker, G.M., 2007. Competitive adsorption of reactive dyes from solution: Equilibrium isotherm studies in single and multisolute systems. Chem. Eng. J. 128, 163–167.

Al-Ghouti, M., Issa, A.A., Al-Saqarat, B.S., Al-Reyahi, A.Y., Al-Degs, Y.S., 2016. Multivariate analysis of competitive adsorption of food dyes by activated pine wood. Desalin. Water Treat. 57, 27651–27662.

Al-Zawahreh, K., Barral, M.T., Al-Degs, Y.S., Paradelo, R., 2021. Comparison of the sorption capacity of basic, acid, direct and reactive dyes by compost in batch conditions. J. Environ. Manag. 294, 113005.

Al-Zawahreh, K., Barral, M.T., Al-Degs, Y.S., Paradelo, R., 2022. Optimization of direct blue 71 sorption by organic rich-compost following multilevel multifactor experimental design. Arab. J. Chem. 15, 103468.

Anastopoulos, I., Kyzas, G.Z., 2015. Composts as biosorbents for decontamination of various pollutants: a review. Water Air Soil Pollut. 226, 61–72.

Ayilara, M., Olanrewaju, O., Babalola, O., Odeyemi, O., 2020. Waste management through composting: Challenges and potentials. Sustainability 12, 4456.

Benkhaya, S., M'rabet, S., El Harfi, A., 2020. Classifications, properties, recent synthesis and applications of azo dyes. Heliyon 6, 03271.

Bilal, M., Rasheed, T., Nabeel, F., Iqbal, H.M.N., Zhao, Y., 2019. Hazardous contaminants in the environment and their laccase-assisted degradation – a review. J. Environ. Manage. 234, 253–264.

Bohart, G.S., Adams, E.Q., 1920. Some aspects of the behavior of charcoal with respect to chlorine. J. Am. Chem. Soc. 42, 523–544.

Chen, G.Q., Zeng, G.M., Tu, X., Niu, C.G., Huang, G.H., Jiang, W., 2006. Application of a byproduct of *Lentinus edodes* to the bioremediation of chromate contaminated water. J. Hazard. Mater. 135 (3), 249–255.

Durai, G., Rajasimman, M., 2011. Biological treatment of tannery wastewater - a review. J. Environ. Sci. Technol. 4, 1–17.

Faust, S.D., Aly, O.M., 1987. Adsorption Processes for Water Treatment. Butterworth Publishers.

Giles, C.H., MacEwan, T.H., Nakhwa, S.N., Smith, D., 1960. Studies in adsorption. Part XI. A system of classification of solution adsorption isotherms, and its use in diagnosis of adsorption mechanisms and in measurement of specific surface areas of solids. J. Chem. Soc. 1960, 3973–3993.

Han, R., Wang, Y., Zhao, X., Wang, Y., Xie, F., Cheng, J., Tang, M., 2009. Adsorption of methylene blue by phoenix tree leaf powder in a fixed-bed column: experiments and prediction of breakthrough curves. Desalination 245 (1–3), 284–297.

Issa, A., Al-Degs, Y.S., El-Sheikh, A.H., Al-Reyahi, A.Y., Al-Bakain, R.Z., Abdelghani, J., Newman, A.P., 2017. Application of partial least squares-kernel calibration in competitive adsorption studies using an effective chemically activated biochar. Clean Soil Air Water 45, e333.

Jóźwiak, T., Filipkowska, U, Rodziewicz, J., Mielcarek, A., Owczarkowska, D., 2013. Application of compost as a cheap sorbent for dyes removal from aqueous solutions. Rocznik Ochrona Srodowiska 15, 2398–2411.

Kamarudzaman, A., Chay, T., Amir, A., Talib, S.A., 2015. Biosorption of Mn(II) ions from aqueous solution by *Pleurotus* spent mushroom compost in a fixed-bed column. Procedia 195, 2709–2716.

Kausar, A., Iqbal, M., Javed, A., Aftab, K., Nazli, Z., Bhatti, H., Nouren, S., 2018. Dyes adsorption using clay and modified clay: A review. J. Mol. Liq. 256, 395–407.

McKay, G., Bion, M.J., 1990. Simplified optimisation for fixed bed adsorption systems. Water Air Soil Pollut. 51, 33–41.

Namasivayam, C., Kumar, M., Selvi, K., Begum, R., Vanathi, T., Yamuna, R., 2001. Waste coir pith—a potential biomass for the treatment of dyeing wastewaters. Biomass Bioenergy 21, 477–483.

Negrea, A., Mihailescu, M., Mosoarca, G., Ciopec, M., Duteanu, N., Negrea, P., Minzatu, V., 2020. Estimation on fixed-bed column parameters of breakthrough behaviors for gold recovery by adsorption onto modified/functionalized amberlite XAD7. Int. J. Environ. Res. Public Health 17, 6868.

Oyekanmi, A., Ahmad, A., Hossain, K., Rafatullah, M., 2019. Adsorption of Rhodamine B dye from aqueous solution onto acid treated banana peel: Response surface methodology, kinetics and isotherm studies. PLoS One 15, e0216878.

Paradelo, R., Al-Zawahreh, K., Barral, M.T., 2020. Utilization of composts for adsorption of methylene blue from aqueous solutions: kinetics and equilibrium studies. Materials 13, e2179.

Paradelo, R., Moldes, A.B., Barral, M.T., 2009. Treatment of red wine vinasses with non-conventional substrates for removing coloured compounds. Water Sci. Technol. 59, 1585–1592.

Paradelo, R., Vecino, X., Moldes, A.B., Barral, M.T., 2019. Potential use of composts and vermicomposts as low-cost adsorbents for dye removal: an overlooked application. Environ. Sci. Pollut. Res. 26, 21085–21097.

Patel, H., 2019. Fixed-bed column adsorption study: a comprehensive review. Appl. Water Sci. 9, 45.

Raval, N.P., Shah, P.U., Shah, N.K., 2017. Malachite green a cationic dye and its removal from aqueous solution by adsorption. Appl. Water Sci. 7, 3407–3445.

Saharimoghaddam, N., Massoudinejad, M., Ghaderpoori, M., 2019. Removal of pollutants (COD, TSS, and NO_3^-) from textile effluent using *Gambusia* fish and *Phragmites australis* in constructed wetlands. Environ. Geochem. Health 41, 1433–1444.

Sharma, D.C., Foster, C.F., 1995. Column studies into the adsorption of chromium (VI) using sphagnum moss peat. Bioresour. Technol. 52 (3), 261–267.

Sy, S., Sofyan, Ardinal, Kasman, M., 2019. Reduction of pollutant parameters in textile dyeing wastewater by gambier (*Uncaria gambir* roxb) using the multi soil layering (MSL) bioreactor. IOP Conf. Ser. Mater. Sci. Eng. 546, 022032.

Tahira, M., Bhatti, H., Iqbal, M., 2016. Solar red and Brittle blue direct dyes adsorption onto *Eucalyptus angophoroides* bark: Equilibrium, kinetics and thermodynamic studies. J. Environ. Chem. Eng. 4, 2431–2439.

Tan, R., Wang, Y., Zhao, X., Wang, Y., Xie, F., Cheng, J., Tang, M., 2008. Adsorption of methylene blue by phoenix tree leaf powder in a fixed-bed column, experiments and prediction of breakthrough curves. Desalination 245 (3), 284–297.

Thomas, H.C., 1944. Heterogeneous ion exchange in a flowing system. J. Am. Chem. Soc. 66, 1664–1667.

Thuong, N., Nhi, N., Nhung, V., Bich, H., Quynh, B., Bach, L., Nguyen, T., 2019. A fixed-bed column study for removal of organic dyes from aqueous solution by pre-treated durian peel waste. Indones. J. Chem. 19 (2), 486–494.

Toptas, A., Demierege, S., Ayan, E.M., Yanik, J., 2014. Spent mushroom compost as biosorbent for dye biosorption. Clean Soil Air Water 42, 1721–1728.

Walker, G.M., Weatherley, L.R., 2000. Textile wastewater treatment using granular activated carbon adsorption in fixed beds. Sep. Sci. Technol. 39, 1329–1341.

Yang, G., Wu, L., Xian, Q., Shen, F., Wu, J., Zhang, Y., 2016. Removal of Congo red and methylene blue from aqueous solutions by vermicompost-derived biochars. PLoS One 11 (5), e0154562.

Yu, Y., Murthy, B., Shapter, J., Constantopoulos, K., Voelcker, N., Ellis, A., 2013. Benzene carboxylic acid derivatized graphene oxide nanosheets on natural zeolites as effective adsorbents for cationic dye removal. J. Hazard. Mater. 260, 330–338.

Yu, J., Zhu, J., Feng, L., Cai, X., Zhang, Y., Chi, R., 2019. Removal of cationic dyes by modified waste biosorbent under continuous model: Competitive adsorption and kinetics. Arab. J. Chem. 12, 2044–2051.